Article

MIMO Underwater Acoustic Communications in Ports and Shallow Waters at Very High Frequency

Gaultier Real [1,†,‡], Pierre-Philippe Beaujean [1,*] and Pierre-Jean Bouvet [2]

[1] Department of Ocean and Mechanical Engineering, Florida Atlantic University,
101 North Beach Road, Dania Beach, FL 33004, USA; E-Mail: real@lma.cnrs-mrs.fr

[2] ISEN Brest, 20 Cuirassé Bretagne, CS 42807, Brest Cedex 2 29228, France;
E-Mail: pierre-jean.bouvet@isen.fr

[†] Current address: Laboratoire de Mécanique et d'Acoustique, CNRS UPR 7051, 31 Chemin Joseph Aiguier, Marseille 13402, France.

[‡] Current address: Thales Underwater Systems SAS, 525 Route des Dolines, BP 157, Sophia-Antipolis Cedex 06903, France.

[*] Author to whom correspondence should be addressed; E-Mail: pbeaujea@fau.edu; Tel.: +1-561-297-0530; Fax: +1-561-297-3885.

Abstract: Hermes is a Single-Input Single-Output (SISO) underwater acoustic modem that achieves very high-bit rate digital communications in ports and shallow waters. Here, the authors study the capability of Hermes to support Multiple-Input-Multiple-Output (MIMO) technology. A least-square channel estimation algorithm is used to evaluate multiple MIMO channel impulse responses at the receiver end. A deconvolution routine is used to separate the messages coming from different sources. This paper covers the performance of both the channel estimation and the MIMO deconvolution processes using either simulated data or field data. The MIMO equalization performance is measured by comparing three relative root mean-squared errors (RMSE), obtained by calculations between the source signal (a pseudo-noise sequence) and the corresponding received MIMO signal at various stages of the deconvolution process; prior to any interference removal, at the output of the Linear Equalization (LE) process and at the output of an interference cancellation process with complete *a priori* knowledge of the transmitted signal. Using the simulated data, the RMSE using LE is −20.5 dB (where 0 dB corresponds to 100% of relative error) while the

lower bound value is −33.4 dB. Using experimental data, the LE performance is −3.3 dB and the lower bound RMSE value is −27 dB.

Keywords: MIMO; underwater; acoustic communications; channel estimation; equalization

1. Introduction

Hermes is a broadband, high-frequency (262 kHz–375 kHz) Under Water Acoustic (UWA) modem designed for very high-bit rate digital communications in ports and shallow waters. In its current form, this modem supports only a single source and a single receiver [1–3]. In this paper, the authors apply Multiple-Input-Multiple-Output (MIMO) technology to Hermes, so that multiple sources and receivers distributed over an area can be used simultaneously. While the channel estimation algorithm (previously presented in [4]) and the MIMO deconvolution technique presented here are well known in the literature [5–7], the important contribution of the paper is to present a performance analysis when applied to high-frequency MIMO data, either simulated or experimental.

MIMO UWA communication is achieved by modifying the signaling of the FAU Hermes uplink message. The limited bandwidth, reliability and flexibility observed with UWA communication systems can be partly resolved by the use of MIMO techniques [5,8–13]. Indeed, the capability to send different messages via each source can significantly increase the overall data rate of the UWA communication system. In addition, the coverage area of the UWA modem can be significantly increased. However, MIMO communication systems cannot guarantee perfect communications, as signal fading; Doppler spread and ambient noise impair the overall performance of any UWA modem [14–16].

The proper retrieval of MIMO messages requires both an accurate estimation of the acoustic channels and an effective channel equalization algorithm. The least-square (LS) channel estimation algorithm was presented in a previous paper [4]. Here, the authors focus on channel deconvolution (MIMO equalization), which is critical to properly separate the messages coming from multiple sources (this is also called co-antenna interference removal) and to remove inter-symbol interference due to acoustic multipath. The deconvolution is implemented as a Minimum Mean Square Error (MMSE) equalizer. The theoretical limit of the deconvolution process is computed with an Interference Cancellation Linear Equalizer (ICLE), which removes the co-antenna interference by using a priori information on the transmitted sequence. Finally, the system performance is studied using simulated data, experimental data and the upper performance bound.

2. System Model

2.1. Source Signals

The messages sent through the acoustic channels are obtained by modifying the signaling of Hermes [1–3]. In this paper, i represents the source index. The proposed message is composed of the source-dependent MIMO sequence $s_{i,h}(t)$ followed after a predefined time delay τ_{msg} with the traditional Hermes message $s_{i,msg}(t)$, such that:

$$s_i(t) = s_{i,h}(t) + s_{i,msg}(t - \tau_{msg})$$ (1)

$s_{i,h}(t)$ consists of perfectly known pseudo noise (PN) sequences of length $\tau = 218.5$ ms, up-sampled from the symbol frequency F_{sym} to the sampling frequency and pulse-shaped using a raised-cosine filter. Figure 1 shows an example of source signal. Given a carrier frequency F_0 and a signal level *SL*, the transmitted signal is

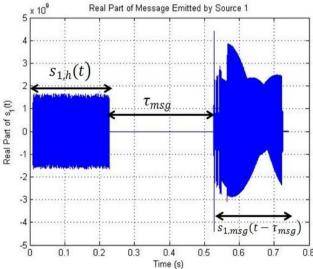$$s_{i,h}(t) = 10^{SL/20} \cdot \left(s_{i,PN}(t) * b_{RC}(t) \right) \cdot \cos\left(2\pi f_0 t \right) \mu Pa$$ (2)

where

$$b_{RC}(t) = \frac{\sin\left(\pi t / T_{sym} \right) + \sin\left(\beta \pi t / T_{sym} \right)}{\left(\pi t / T_{sym} \right)\left(1 - 4\left(\beta t / T_{sym} \right)^2 \right)}$$ (3)

here, β is the roll-off coefficient and T_{sym} is the symbol period.

Figure 1. Real part of source message 1.

In this paper, we assume that the message following the MIMO sequence does not change with the source. The MIMO sequences (one per source) have a very low cross-correlation to their auto-correlation peak ratio. We observed that the peak ratio is approximately 40 (which is equivalent to 16 dB).

2.2. Received Signals

In this section, we present the operations carried out at the receiver end. We first focus on the channel estimation algorithm, followed by the equalization. The derivations are provided in the discrete time domain, where k stands for the time index and l the delay index.
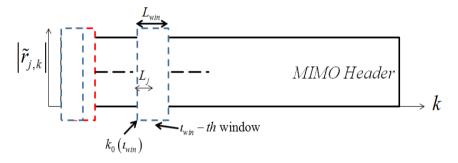
2.2.1. Channel Estimation

This process is performed over the duration of N_{win} time windows, of time index t_{win} and length L_{win}. The received samples $\tilde{\mathbf{r}}_j$ at receiver j can be written in matrix form [4,17]:

$$\tilde{\mathbf{r}}_j = \mathbf{S}_j \tilde{\mathbf{h}}_j + \tilde{\mathbf{n}}_j \qquad (4)$$

where $\mathbf{S}_j \in \mathbb{R}^{(L_{win}-L_j)\times T_j}$ represents the augmented source signal array at the j th receiver. $\mathbf{h}_j \in \mathbb{C}^{(T_j)\times 1}$ represents the augmented channel impulse response array. $\tilde{\mathbf{n}}_j \in \mathbb{C}^{(L_{win}-L_j+1)\times 1}$ represents the noise array.

As depicted in Figure 2, $k_0(t_{win})$ denotes the beginning of the time window. L_{ij} is the length of the channel impulse response between transmitter i and receiver j, and $L_j = \max_{i\in[1;N_t]}\{L_{ij}\}$. Finally, T_j is the sum of the channel lengths over the total number of transmitters N_t, so that $T_j = \sum_{i=1}^{N_t} L_{ij}$.

Figure 2. Definition of the parameters of the time-window used to perform the channel estimation at receiver j.

In the continuous time domain, the quantity T_j is noted T_L (this term is also used in the results section). The index j must be dropped, as the tunable parameter T_L is assumed identical across every receiver. We study the influence of this parameter on channel estimation and deconvolution in the results section. The channel estimation is performed through minimization of the following quantity [18],

$$\tilde{\mathbf{h}}_j^{est} = \arg\min_{\tilde{\mathbf{h}}_j} \left\| \tilde{\mathbf{r}}_j - \mathbf{S}_j \tilde{\mathbf{h}}_j \right\|^2 \qquad (5)$$

This leads to the LS estimation of $\tilde{\mathbf{h}}_j$ for every time window index t_{win},

$$\tilde{\mathbf{h}}_j^{est} = \left(\mathbf{S}_j^H \mathbf{S}_j\right)^{-1} \mathbf{S}_j^H \tilde{\mathbf{r}}_j \qquad (6)$$

where $(\ )^H$ represents the Hermitian operator. This operation requires a $T_j \times T_j$ matrix inversion.

2.2.2. MIMO Deconvolution

The MIMO deconvolution process presented in this paper compensates for co-channel and inter-symbol interferences using the LS channel estimation obtained in Equation (6). The critical parameters identified in this performance study are: (1) the length of the channel estimate T_L; (2) the length T_k of the pre-cursor and post-cursor of the linear equalization filter. We consider two equalization structures: conventional Linear Equalization (LE) and Interference Cancellation Linear Equalization (ICLE). ICLE provides a theoretical lower bound of the equalization process.

2.2.2.1. Minimum Mean Squared Error Linear Equalization

The process presented in this section consists of a feed-forward multi-channel linear filter optimized under MMSE criterion. Let L represent the maximum value of the sub-channel length L_{ij},

$$L = \max_{i \in [1;N_t], j \in [1;N_r]} \{L_{ij}\} \tag{7}$$

We define the matrices $\breve{\mathbf{r}}_k \in \mathbb{C}^{N_r}$ and $\breve{\mathbf{n}}_k \in \mathbb{C}^{N_r}$ as the received signal and noise over the total number of hydrophones:

$$\breve{\mathbf{r}}_k = \left[\tilde{r}_{1,k}, \cdots, \tilde{r}_{N_r,k} \right]^T \tag{8}$$

and

$$\breve{\mathbf{n}}_k = \left[\tilde{n}_{1,k}, \cdots, \tilde{n}_{N_r,k} \right]^T \tag{9}$$

Similarly, we define the transmitted signals $\mathbf{s}_k \in \mathbb{R}^{N_t}$ and channel impulse responses $\mathbf{H}_l \in \mathbb{C}^{N_r \times N_t}$ as:

$$\mathbf{s}_k = \left[s_{1,k}, \cdots, s_{N_t,k} \right]^T \tag{10}$$

$$\mathbf{H}_l = \begin{bmatrix} \tilde{h}_{11,l} & \tilde{h}_{21,l} & \cdots & \tilde{h}_{N_t 1,l} \\ \vdots & & & \vdots \\ \tilde{h}_{1N_r,l} & \tilde{h}_{2N_r,l} & \cdots & \tilde{h}_{N_t N_r,l} \end{bmatrix} \tag{11}$$

Therefore, the received signal becomes

$$\breve{\mathbf{r}}_k = \sum_{l=0}^{L-1} \mathbf{H}_l \mathbf{s}_{k-l} + \breve{\mathbf{n}}_k \tag{12}$$
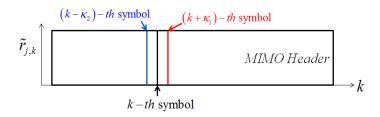
We now define κ_1 and κ_2 (Figure 3) as the pre-cursor and post-cursors of the linear equalization filter. In this case, $\mathbf{x}_k \in \mathbb{R}^{(L+\kappa_1+\kappa_2)N_t}$, $\mathbf{y}_k \in \mathbb{C}^{(1+\kappa_1+\kappa_2)N_r}$ and $\mathbf{w}_k \in \mathbb{C}^{(1+\kappa_1+\kappa_2)N_r}$ are defined as

$$\mathbf{x}_k = \left[\mathbf{s}_{k-\kappa_2-L+1}^T, \cdots, \mathbf{s}_{k+\kappa_1}^T \right]^T \tag{13}$$

$$\mathbf{y}_k = \left[\breve{\mathbf{r}}_{k-\kappa_2}^T, \cdots, \breve{\mathbf{r}}_{k+\kappa_1}^T \right]^T \tag{14}$$

$$\mathbf{w}_k = \left[\breve{\mathbf{n}}_{k-\kappa_2}^T, \cdots, \breve{\mathbf{n}}_{k+\kappa_1}^T \right]^T \tag{15}$$

Figure 3. Multiple-Input-Multiple-Output (MIMO) deconvolution process: pre-cursor and post-cursor definition.

In the results section, the influence of the pre-cursor and post-cursor is studied in the continuous time domain. In this paper, the length of these cursors is assumed to be the same and is represented by T_k. Next, we define the augmented matrix containing the matrices of channel impulse responses, denoted $\mathbf{H} \in \mathbb{C}^{((1+\kappa_1+\kappa_2)N_r) \times ((L+\kappa_1+\kappa_2)N_t)}$,

$$\mathbf{H} = \begin{bmatrix} \mathbf{H}_{L-1} & \cdots & \mathbf{H}_0 & 0 \\ & \ddots & & \ddots \\ 0 & \mathbf{H}_{L-1} & \cdots & \mathbf{H}_0 \end{bmatrix} \tag{16}$$

so that

$$\mathbf{y}_k = \mathbf{H}\mathbf{x}_k + \mathbf{w}_k \tag{17}$$

The output of LE process can be expressed as:

$$u_{i,k}^{est} = \mathbf{c}_i^T \mathbf{y}_k \tag{18}$$

In the sense of the MMSE criterion without any a priori on transmitted symbols, the optimum equalization filter is [5,18],

$$\mathbf{c}_i = \left(\hat{\mathbf{H}}\hat{\mathbf{H}}^H + \frac{\sigma_n^2}{\sigma_s^2}\mathbf{I} \right)^{-1} \hat{\mathbf{H}}\mathbf{e}_{((\kappa_2-1+L)N_t+i)} \tag{19}$$

where $\mathbf{I}$ is the identity matrix of size $(1+\kappa_1+\kappa_2)N_r$, σ_n^2 is the variance of the noise and σ_s^2 is the variance of the original sequence $s_{i,k}$. $\mathbf{e}_{((\kappa_2-1+L)N_t+i)}$ denotes a column vector of size $(L+\kappa_1+\kappa_2)N_t$ with 1 at index i and 0 at other positions. $\hat{\mathbf{H}} \in \mathbb{C}^{(1+\kappa_1+\kappa_2)N_r \times (L+\kappa_1+\kappa_2)N_t}$ is the estimates of augmented channel matrix H or time window index t_{win} Here, the estimated signal $s_{i,k}^{est}$ depends on length of the time window, which in turns depends on the measured channel response. If $N_{win} = 1$, the channel is stationary over a message duration and

$$s_{i,k}^{est} = u_{i,k}^{est} \tag{20}$$

However, if $N_{win} \geq 1$, $u_{i,k}^{est}$ becomes a function of t_{win}. In this case, the equalized signal for each sliding window is cropped and forms a section of the equalized output $s_{i,k}^{est}$,

$$s_{i,k'}^{est} = u_{i,k}^{est}, \text{ where } \frac{L_{win}}{4} \leq k \leq \frac{3L_{win}}{4} - 1, \ k' = k + (\iota_{win}-1)L_{win}O_R \text{ and } 1 \leq \iota_{win} \leq N_{win} - 2 \tag{21}$$

The variables t_{win}, L_{win} and O_R represent the time window index, length and overlapping rate, respectively.

2.2.2.2. MMSE Interference Cancellation Linear Equalizer

The ICLE has been developed to evaluate the best possible performance of the deconvolution process by assuming that the source signal is perfectly known. The output of the ICLE may be expressed as follows [6,7,19],

$$u_{i,k}^{ICLE} = \mathbf{p}_{i,k}^H \mathbf{y}_k - \mathbf{q}_{i,k}^H \bar{\mathbf{v}}_{i,k} \tag{22}$$

$\mathbf{y}_k$ is defined in Equation (17). $\mathbf{p}_{i,k}$ and $\mathbf{q}_{i,k}$ respectively stand for the feed-forward and feed-back filters. $\bar{\mathbf{v}}_{i,k}$ is defined as

$$\bar{\mathbf{v}}_{i,k} = \left[s^T_{k-N_{ICLE}-L+2}, \cdots, s^T_{k-K_{ICLE}-1}, \mathbf{v}^T_{i,k-K_{ICLE}}, s^T_{k-K_{ICLE}+1}, \cdots, s^T_k \right]^T \tag{23}$$

where,

$$\mathbf{v}^T_{i,k} = \left[s_{1,k}, \cdots, s_{i-1,k}, 0, s_{i+1,k}, \cdots, s_{N_t,k} \right]^T \tag{24}$$

K_{ICLE} is the discrete delay index induced by the equalizer, such that $0 \le K_{ICLE} \le N_{ICLE} + L - 2$, where N_{ICLE} represents the discrete ICLE length. Under MMSE optimization, the feed-forward and feed-back equalization vectors become equal to [7]:

$$\begin{cases} \mathbf{p}_{i,k} = \lambda_k \bar{\mathbf{p}}_k \\ \mathbf{q}_{i,k} = \hat{\mathbf{H}}^H \mathbf{p}_k \end{cases} \tag{25}$$

where

$$\lambda_k = \frac{1}{1 + \mathbf{e}^T_{i,N_{ICLE}+L-1-K_{ICLE}} \hat{\mathbf{H}}^H \bar{\mathbf{p}}_k} \tag{26}$$

and

$$\bar{\mathbf{p}}_k = \frac{\sigma^2_s}{\sigma^2_n} \hat{\mathbf{H}} \mathbf{e}_{i,N_{ICLE}+L-1-K_{ICLE}} \tag{27}$$

$\mathbf{e}_{i,k}$ is a null column vector, with the exception of element $N_t(k-1) + i$ equal to 1. σ^2_n represents the noise variance. The ICLE estimate $s^{ICLE}_{i,k}$ depend on the number of time windows used to perform the channel estimation, thus Equations (23)–(25) also apply to $s^{ICLE}_{i,k}$.

3. Simulated and Experimental Results

The results, in terms of MIMO deconvolution, are presented in this section. The simulation parameters and the metrics are first presented, followed with a description of the experimental setup. The simulated results are analyzed: in this case, the channel is stationary over the duration of the message. Finally, a set of field data is analyzed, where time variations of the channel are observed.

3.1. Experimental Setup

A series of experiments was carried out in the Florida Atlantic University Seatech marina (Figure 4). While the experimental setup presented here uses two sources and three receivers, this paper presents only the results obtained with two receivers. Table 1 provides a summary of the data collection. A first set of data was acquired on 27 September 2011. A second series of experiments took place on 31 August 2011. The two sources were alternatively placed at the two locations labeled "Pos1" and "Pos7" in Figure 4. Two splash proof boxes were built to prevent any damage to the modem sources and were installed on kayaks. Each box contained a set of Hermes source electronics, an ITC-1089

source transducer and a battery pack. The source level was 179 dB ref. 1 μPa at 1 m. The receivers used to carry out these missions were deployed off a small research vessel. The experimental ranges are given in Table 2. The signals presented in this paper were acquired at a maximum range of 27 m. This short range is mostly due to the high sound absorption loss (100 dB/km at 20 ℃ and at 300 kHz [20]).

Since the equipment did not have the ability to perform real-time MIMO communication, each source was used individually and the MIMO messages were constructed off-line. The signal-to-noise ratio SNR_j was calculated at each receiver j. The value of SNR_j, averaged across every messages within a mission, is shown in Table 3. The observed SNR value varied between 27.1 dB and 34.3 dB from mission to mission. These variations are mostly due to the time varying characteristics of the channel, which dramatically impacts the average power of the received signals.

Figure 4. Experimental setup.

Table 1. Summary of data collected.

Mission Number and Date	Source 1 Position	Source 2 Position	Receiver 1 Position	Receiver 2 Position	Number of Messages Retained
1-07/27/2011	Pos1	Pos7	Rx1	Rx3	50
2-07/27/2011	Pos7	Pos1	Rx1	Rx3	50
3-08/29/2011	Pos7	Pos1	Rx1	Rx3	100
4-08/29/2011	Pos1	Pos7	Rx1	Rx3	100

Table 2. Experimental ranges.

Distance on Figure 4	Distance (m)
Rx1-Pos1	24
Rx1-Pos7	27
Rx3-Pos1	23.3
Rx3-Pos7	25.8
Pos1-Pos7	6.15
Rx1-Rx3	2.68

Table 3. Signal-to-noise ratio per mission and per receiver.

Mission Number and Date	SNR$_1$(dB)	SNR$_2$(dB)
1-07/27/2011	27.1	27.3
2-07/27/2011	28.8	27.8
3-08/29/2011	30.9	34.3
4-08/29/2011	29.2	33.2

3.2. Simulation Parameters

The channel model, presented in detail in [4,17], combines a deterministic model (to determine the average echo intensities) [15,16] and a stochastic Rician model (to add some random fluctuation to every echo intensity) [4]. Sources and receivers' separation and depth match the experimental setup presented in Section 3.1.

The simulation parameters (Table 4) are tuned to match the experimental data sets as closely as possible. Doppler shift and Doppler spread have been derived from the field data. The time window used to perform the channel estimation covers the duration of the MIMO sequence and the dead-time interval. Hence, the channel is assumed to be time-invariant over the transmission of a message. The coherence time of the channel therefore corresponds to the total length of the transmitted message: each new transmission would lead to a different channel to estimate.

For every transmitted message, we also adjust the time delay τ_0 between the signals measured at every receiver. In this paper, we only consider full overlap between received messages. The results for partial overlap are presented in [17]. The channel model considered here includes both the specular reflection from the sea bottom and scattering from the sea surface and bottom.

Table 4. Simulation parameters. Some of the simulation parameters are not formally used in the equations listed in this paper. The parameter name is followed with references [4,17], where the equations using these parameters are provided.

Name	Symbol	Value (units)	Name	Symbol	Value (units)
Sources Depth [4,17]	D_{Si}	1 m	Source Level	SL	179 dB re 1 µPa @ 1 m
Receivers Depth [4,17]	D_{Rj}	1.5 m	Noise Level	NL	83.7 dB re 1 µPa
Water Depth [4,17]	D_W	3 m	Sampling Frequency	F_S	150 kHz in base band 750 kHz in pass band
Water Sound Speed [4,17]	c	1,500 m/s	Symbol Rate	D_{sym}	75 kHz
Water Density [4,17]	ρ	1,023 kg/m^3	Carrier Frequency	f_0	0 kHz in base band 300 kHz in pass band
Sandy Sediment Sound Speed [4,17]	c_b	1,800 m/s	MIMO Sequence Duration	τ_h	218.5 ms
Sandy Sediment Density [4,17]	ρ_b	1,800 kg/m^3	Dead-Time Duration	τ_{msg}	300 ms

Table 4. *Cont.*

Name	Symbol	Value (units)	Name	Symbol	Value (units)
Sea Bottom Loss [4,17]	L_{SB}	5 dB	Correlation Threshold Parameter	K_{thr}	20
Beginning of Time Window [4,17]	k_0	0	Time Window Length	τ_{win}	518.5 ms
Number of Transmitters [4,17]	N_t	2	Number of Receivers	N_r	2
Distance Source 1 Receiver 1 [4,17]	R_{11}	23.3 m	Distance Source 1 Receiver 2 [4,17]	R_{12}	24 m
Distance Source 2 Receiver 1 [4,17]	R_{21}	25.8 m	Distance Source 2 Receiver 2 [4,17]	R_{22}	27 m

3.3. Performance Metrics

First, we present the performance of the channel estimation process. This performance is measured using the RMSE between the received MIMO header and the MIMO header convolved with the estimated channel, averaged across every message m and every receiver j [17]:

$$\text{RMSE}_{CE}\left(dB\right) = 20\log_{10}\left(\sqrt{\frac{\dfrac{\sum_{j=1}^{N_r}\sum_{m=1}^{N_{msg}}\left\|\tilde{\mathbf{r}}_j - \mathbf{S}_j\tilde{\mathbf{h}}_j^{est}\right\|^2}{N_r L N_{msg}}}{\dfrac{\sum_{j=1}^{N_r}\sum_{m=1}^{N_{msg}}\left|\tilde{r}_j\left(t_m\right)\right|^2}{N_r N_{msg}}}}\right) \tag{28}$$

The MIMO LE performance is measured using the relative RMSE between the deconvolved MIMO header and the original sequence. This metric indicates the accuracy of the co-antenna and inter-symbol interference removal process. In this case, the RMSE is given by [17]:

$$\text{RMSE}_{MIMO\_LE}\left(dB\right) = 20\log_{10}\left(\sqrt{\frac{\dfrac{\sum_{i=1}^{N_t}\sum_{m=1}^{N_{msg}}\sum_{k_m=\kappa_1+L}^{L_h-\kappa_2}\left|s_i^{est}\left(k_m\right)-s_i\left(k_m\right)\right|^2}{N_t N_{msg}\left(L_h-\left(\kappa_2+\kappa_1+L\right)\right)}}{\dfrac{\sum_{i=1}^{N_t}\sum_{m=1}^{N_{msg}}\sum_{k_m=\kappa_1+L}^{L_h-\kappa_2}\left|s_i\left(k_m\right)\right|^2}{N_t N_{msg}\left(L_h-\left(\kappa_2+\kappa_1+L\right)\right)}}}\right) \tag{29}$$

In order to evaluate the impact of the linear equalization on the received signals, RMSE_{MIMO_LE} is compared to another relative RMSE between emitted and raw received signals. This second metric is calculated by comparing the received MIMO header signal (prior to any interference removal) and the corresponding source signal [17]:

$$\text{RMSE}_{MIMO\_Raw}\left(dB\right) = 20\log_{10}\left(\sqrt{\frac{\dfrac{\sum\limits_{i=1}^{N_t}\sum\limits_{m=1}^{N_{msg}}\sum\limits_{k_m=\kappa_1+L}^{L_h-\kappa_2}\left|\tilde{r}_i\left(k_m\right)-s_i\left(k_m\right)\right|^2}{N_t N_{msg}\left(L_h-\left(\kappa_2+\kappa_1+L\right)\right)}}{\dfrac{\sum\limits_{i=1}^{N_t}\sum\limits_{m=1}^{N_{msg}}\sum\limits_{k_m=\kappa_1+L}^{L_h-\kappa_2}\left|s_i\left(k_m\right)\right|^2}{N_t N_{msg}\left(L_h-\left(\kappa_2+\kappa_1+L\right)\right)}}}\right) \tag{30}$$

The performance estimated with the ICLE represents the theoretical performance limit of the MIMO LE. The relative RMSE between emitted MIMO sequences and the output of the ICLE is [17]:

$$\text{RMSE}_{MIMO\_ICLE}\left(dB\right) = 20\log_{10}\left(\sqrt{\frac{\dfrac{\sum\limits_{i=1}^{N_t}\sum\limits_{m=1}^{N_{msg}}\sum\limits_{k_m=N_{ICLE}+K_{ICLE}}^{L_h-K_{ICLE}}\left|s_i^{ICLE}\left(k_m\right)-s_i\left(k_m\right)\right|^2}{N_t N_{msg}\left(L_h-\left(N_{ICLE}+2K_{ICLE}\right)\right)}}{\dfrac{\sum\limits_{i=1}^{N_t}\sum\limits_{m=1}^{N_{msg}}\sum\limits_{k_m=N_{ICLE}+K_{ICLE}}^{L_h-K_{ICLE}}\left|s_i\left(k_m\right)\right|^2}{N_t N_{msg}\left(L_h-\left(N_{ICLE}+2K_{ICLE}\right)\right)}}}\right) \tag{31}$$

3.4. MIMO Channel Estimation Results

Table 5 shows the values of RMSE_{CE} *as* a function of T_L for both experimental and simulated data. The maximum value of T_L is 5.33 ms, as higher values of T_L lead to singularities and does not produce accurate results. As a reminder, RMSE_{CE} measures the error between the received signals and the emitted sequences convolved with the estimated channels. RMSE_{CE} is averaged across every receiver, so that the results presented in Table 5 translate the accuracy of the channel estimation across every sub-channel.
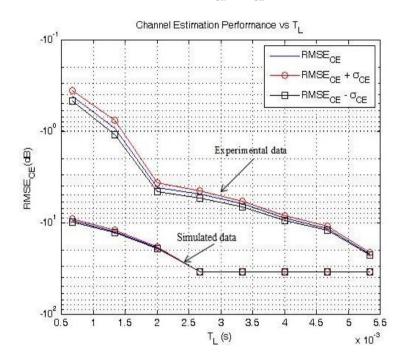
Table 5. Relative root mean-squared errors (RMSE_{CE}) as a function of T_L.

T_L(ms)	**Simulated** RMSE_{CE} *(dB)*	**Experimental** *$RMSE_{CE}$ (dB)*
0.667	−9.5	−0.4
1.333	−12.5	−0.9
2.0	−18.8	−4.1
2.667	−34.7	−4.9
3.333	−34.7	−6.2
4.0	−34.7	−9.1
4.667	−34.8	−11.4
5.33	−34.8	−25.7

In both experimental and simulation cases, as T_L increases, the accuracy of the channel estimation improves. However, while RMSE_{CE} reaches a sweet-spot at $T_L = 2.667$ ms using simulated data ($\text{RMSE}_{CE} \simeq -34.7$ dB), the experimental results on RMSE_{CE} differ. Indeed, the minimum RMSE_{CE} is obtained for $T_L = 5.33$ ms ($\text{RMSE}_{CE} = -25.7$ dB) as shown in Table 5 and Figure 5. If, as explained earlier on, values higher than $T_L = 5.33$ ms cannot be considered, the minimum value of RMSE_{CE} using

experimental data is of the same order of magnitude as RMSE_{CE} in the simulation framework. The channel estimation can therefore be considered as very accurate.

Figure 5 displays the influence of T_L on the channel estimation accuracy in the specific case of mission 4. Figure 6 shows that RMSE_{CE} drops and the confidence interval $\left[-\sigma_{CE};\sigma_{CE}\right]$ gets narrower as T_L increases.

Figure 5. RMSE_{CE} and $\text{RMSE}_{CE} \pm \sigma_{CE}$ as a function of T_L.

The SNR is simply computed as the ratio of the received MIMO header power over the ambient noise power. It is also interesting to look at the impact of the SNR on the channel estimation performance for every receiver and every mission carried out. The best possible estimation of the channel impulse response is obtained when RMSE_{CE} at the output of the channel estimator (Equation (28)) is the inverse of the SNR. In this ideal case, the relationship can be rewritten in dB,

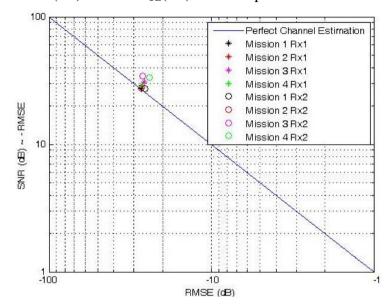$$SNR\left(dB\right) = -RMSE_{CE}\left(dB\right) \tag{32}$$

where the SNR is simply computed as the ratio of the received MIMO header power over the ambient noise power.

In the more realistic case of imperfect channel estimation, Equation (4) should account for the residual error in estimating the channel impulse response at receiver j. This error can be modeled as an additive noise $\tilde{\boldsymbol{\xi}}_j$, such that:

$$\tilde{\mathbf{r}}_j = \mathbf{S}_j\tilde{\mathbf{h}}_j + \tilde{\mathbf{n}}_j + \tilde{\boldsymbol{\xi}}_j \tag{33}$$

We can verify the validity of such an approximation by comparing the SNR as shown in Table 2 and the RMSE_{CE}(dB) (Equation (28)) obtained for each of the corresponding four missions and for each receiver. In theory, when the best possible estimation of the channel impulse response is calculated, Equation (32) applies, as shown using a solid line in Figure 6. The experimental results, labeled as individual points in Figure 6, remain very close to this theoretical limit, which indicates that

the channel estimation algorithm works very well indeed. For example, the channel estimation in the data set recorded during in mission 2 at receiver 2 results in a value of RMSE$_{CE}$ (dB) that is almost exactly the opposite of *SNR(dB)*. Some discrepancies are also observed, as in mission 3 at receiver 2. In this case, the channel estimator produces significant amounts of additive noise.

Figure 6. *SNR*(dB) *vs.* *RMSE$_{CE}$*(dB) at the output of the channel estimator.

3.5. MIMO Deconvolution Results

A comparison of the MIMO deconvolution capability between experimental data and simulation results has been completed, using the metrics defined in Equations (29)–(31). The results are shown in Tables 6 and 7. The impact of the parameter T_L on the performance metrics is clearly observed. The results are shown for $T_\kappa = T_{\kappa_{max}} = 6$ ms , which lead to the lowest RMSE values [17]. Both simulations and experimental results (averaged over the total number of missions carried out) are presented in Table 6. Clearly, RMSE$_{MIMO\_LE}$ and RMSE$_{MIMO\_ICLE}$ decrease as T_L increases using either simulated or field data. Note that the equalizer length is limited to $T_L = 5.33$ ms, as higher values of T_L led to singularities.

RMSE$_{MIMO\_LE}$, computed with both simulated and experimental data, is shown in Figure 7. Figure 7 shows the influence of the pre-cursor and post-cursor length: if T_L is sufficiently large to provide accurate channel estimation, RMSE$_{MIMO\_LE}$ drops as T_κ increasing. Therefore, showing the influence of T_L on RMSE$_{MIMO\_LE}$ is not of great interest: this is why we chose to represent RMSE$_{MIMO\_LE}$ as a function of T_κ only ($T_L = 5.33$ ms). For example, for an equalizer length $T_L = 5.33$ ms, RMSE$_{MIMO\_LE} = -6.2$ dB with $T_\kappa = 0.7$ ms and drops to RMSE$_{MIMO\_LE} = -20.5$ dB with $T_\kappa = 6.0$ ms . As it has been shown in the channel estimation process results, the confidence interval also narrows as the process gets more and more reliable.
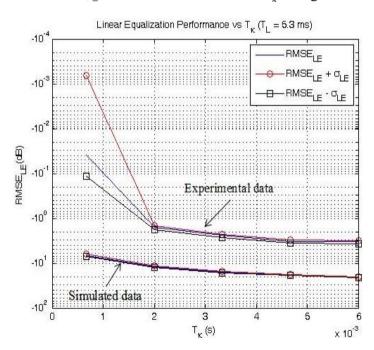
Table 6. RMSE between emitted and (Raw) received signals, RMSE$_{MIMO\_Raw}$ as a function of T_L.

T_L (ms)	RMSE$_{MIMO\_Raw}$ (dB)	
	Simulations	**Experiments**
0.667 ms, 1.333 ms, 2 ms, 2.667 ms, 3.333 ms, 4 ms, 4.667 ms, 5.33 ms	0.04	3

Table 7. RMSE between emitted and received Signals after LE processing, RMSE$_{MIMO\_LE}$ and after ICLE processing, RMSE$_{MIMO\_ICLE}$ as functions of T_L.
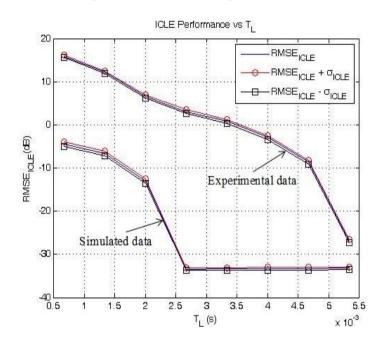
		RMSE$_{MIMO\_Raw}$ (dB)		RMSE$_{MIMO\_ICLE}$ (dB)	
		Simulations	**Experiments**	**Simulations**	**Experiments**
	0.667	0.4	19.7	−4.5	15.8
	1.333	−3.4	14.4	−6.7	12.1
	2.0	−10.3	8.3	−13	6.4
	2.667	−20.5	5.5	−33.4	3.1
T_L (ms)	3.333	−20.5	2.2	−33.4	0.7
	4.0	−20.5	−1.9	−33.3	−3
	4.667	−20.5	−3.9	−33.3	−8.8
	5.33	−20.5	−3.3	−33.2	−26.9

Figure 7. RMSE$_{MIMO\_LE}$ as a function of T_L and T_κ using simulated data.

In the case of experimental data, severe distortions in the received signals impact the accuracy of the MIMO deconvolution process. Indeed, $T_\kappa = 6.0$ ms varies dramatically when computed with simulation and experimental data. In the best case scenario, we use $T_L = 5.33$ ms and $T_\kappa = 6$ ms . Table 7 shows that RMSE$_{MIMO\_LE}$ = −3.9 dB using real data *vs.* RMSE$_{MIMO\_LE}$ = −20.5 dB using simulated data. Nevertheless, the LE process on experimental data dramatically improves the quality of the received signal: Table 6 shows that RMSE$_{MIMO\_Raw}$ = 3 dB whereas Table 7 shows that RMSE$_{MIMO\_LE}$ = −3.3 dB when $T_L = 5.33$ ms.

The relatively significant differences between simulation and field data performances are related to the time-varying characteristics of the experimental channel but also to co-antenna interferences.

Indeed, the experimental channel impulse responses presented a coherence time much shorter than in the simulation case, leading to a lack of accuracy in the co-antenna interference removal process. Figure 8 shows the variation of RMSE_{MIMO_ICLE} as a function of T_L: if the MIMO sequence is known, the accuracy of the process improves as T_L increases. On average, $\text{RMSE}_{MIMO\_ICLE} = -26.9$ dB when $T_L = 5.33$ ms using experimental data *vs.* -33.2 dB using simulated data.

Figure 8. RMSE_{MIMO_ICLE} and $\text{RMSE}_{MIMO\_ICLE} \pm \sigma_{ICLE}$ as a function of T_L.

As expected, the comparisons between RMSE_{MIMO_ICLE} and RMSE_{MIMO_LE} calculated using simulated and experimental data reveals that LE process does not reach the lower bound provided by ICLE structure. Using simulation data, we find that $\text{RMSE}_{MIMO\_ICLE} = -33.2$ dB while $\text{RMSE}_{MIMO\_LE} = -20.5$ dB. This phenomenon is especially pronounced in the case of experimental data, where $\text{RMSE}_{MIMO\_ICLE} = -26.9$ dB and $\text{RMSE}_{MIMO\_LE} = -3.3$ dB for $T_L = 5.33$ ms. One can conclude that LE alone is not totally sufficient to remove the whole interference terms provided by the frequency selective channel and multi-antenna architecture. Non-linear approaches like iterative processing strategy or decision feedback equalization appear thus necessary.

4. Conclusions

The capability of Hermes to support MIMO technology was presented in this paper. The system performance was evaluated using both simulated and experimental data, using two sources and two receivers. The ability to retrieve emitted messages, using a Linear Equalizer (LE), in the presence of inter-symbol interferences, co-antenna interferences and noise was estimated.

The channel impulse response estimation performance was related to the value of the channel estimate length T_L. Computer simulations showed that for $T_L \geq 2.667$ ms, the relative root mean-square error used to measure the accuracy of the estimation reached a plateau. In this configuration, the RMSE (labeled $\text{RMSE}_{CE}(dB)$) between the received MIMO header and the MIMO header convolved with the estimated channel (averaged across every message and every receiver) was

equal to −34.8 dB. This performance was compared to experimental data: in this case the same metric was equal to −25.7 dB for T_L = 5.33 ms, indicating that the proposed technique evaluated fairly accurately the acoustic channel between every source and receiver.

To measure the benefits of this linear equalizer, the RMSE between emitted and received messages was first computed for each individual source and receiver. An Interference Cancelation Linear Equalizer (ICLE) was also developed to measure the limit of the deconvolution process, using estimated channel impulse responses. Optimized under the MMSE criterion, the ICLE took advantage of the known source signal. Using simulated data, T_L = 5.33 ms and $T_\kappa = 6$ ms , the RMSE was estimated at 0.03 dB before equalization (labeled RMSE$_{MIMO\_Raw}$ (dB)), −20.5 dB after LE (labeled RMSE$_{MIMO\_LE}$ (dB)) and −33.3 dB after ICLE (labeled RMSE$_{MIMO\_ICLE}$ (dB)). For experimental data (with the same values for T_L and T_κ), the RMSE was estimated at −3 dB before equalization, −3.3 dB after LE and to −26.9 dB after ICLE.

To conclude with the results presented in this paper, the channel estimator and ICLE processes produce fairly similar results in simulation and experimentations. The fact that the performance of the channel estimation process and the ICLE are very comparable indicates that the deconvolution process is very accurate; in this case, the residual errors are not due to the ICLE itself. The LE performs better with simulated data but still brings some benefits to the communication system in the case of field data. The encouraging results indicate that the FAU Hermes underwater acoustic modem could be successfully equipped with MIMO technology.

Acknowledgments

Conflicts of Interest

The authors declare no conflict of interest.

References

1. Beaujean, P.P.J.; Carlson, E.A. HERMES a high bit-rate underwater acoustic modem operating at high frequencies for ports and shallow water applications. *Mar. Technol. Soc. J.* **2009**, *43*, 21–32.
2. Beaujean, P.P.; Carlson, E. Combined Vehicle Control, Status Check and High-Resolution Acoustic Images Retrieval Using a High-Frequency Acoustic Modem on a Hovering AUV. In Proceedings of OCEANS 2010, Seattle, WA, USA, 20–23 September 2010; pp. 1–10.
3. Beaujean, P.P. A Performance Study of the High-Speed, High-Frequency Acoustic Uplink of the Hermes Underwater Acoustic Modem. In Proceedings of OCEANS 2009-EUROPE, Bremen, Germany, 11–14 May 2009; pp. 1–6.
4. Real, G.; Beaujean, P.P.; Bouvet, P.J. A Channel Model and Estimation Technique for MIMO Underwater Acoustic Communications in Ports and Very Shallow Waters at very High Frequencies. In Proceeding of OCEANS 2011, Waikoloa, HI, USA, 19–22 September 2011; pp. 1–9.

5. Tao, J.; Zheng, Y.R.; Xiao, C.; Yang, T.C.; Yang, W.B. Time-Domain Receiver Design for MIMO Underwater Acoustic Communications. In Proceedings of OCEANS 2008, Quebec City, QC, USA, 15–18 September 2008; pp. 1–6.

6. Tuchler, M.; Singer, A.C.; Koetter, R. Minimum mean squared error equalization using a priori information. *IEEE Trans. Signal Process.* **2002**, *50*, 673–683.

7. Bouvet, P.J.; Héard, M.; le Nir, V. Simple iterative receivers for MIMO LP-OFDM systems. In *Annales des telecommunications*; Springer-Verlag: Berlin, Germany, 2006; Volume 61, pp. 578–601.

8. Bouvet, P.J.; Loussert, A. Capacity Analysis of Underwater Acoustic MIMO Communications. In Proceedings of OCEANS 2010 IEEE-Sydney, Sydney, Australia, 24–27 May 2010; pp. 1–8.

9. Kilfoyle, D.B.; Preisig, J.C.; Baggeroer, A.B. Spatial modulation experiments in the underwater acoustic channel. *IEEE J. Ocean. Eng.* **2005**, *30*, 406–415.

10. Roy, S.; Duman, T.M.; McDonald, V.; Proakis, J.G. High-rate communication for underwater acoustic channels using multiple transmitters. *IEEE J. Ocean. Eng.* **2007**, *32*, 663–688.

11. Li, B.; Huang, J.; Zhou, S.; Ball, K.; Stojanovic, M.; Freitag, L.; Willett, P. MIMO-OFDM for high-rate underwater acoustic communications. *IEEE J. Ocean. Eng.* **2009**, *34*, 634–644.

12. Ceballos Carrascosa, P.; Stojanovic, M. Adaptive channel estimation and data detection for underwater acoustic MIMO-OFDM systems. *IEEE J. Ocean. Eng.* **2010**, *35*, 635–646.

13. Song, A.; Badiey, M. Time reversal multiple-input/multiple-output acoustic communication enhanced by parallel interference cancellation. *J. Acoust. Soc. Am.* **2012**, *131*, 281–291.

14. Stojanovic, M.; Catipovic, J.A.; Proakis, J.G. Phase-coherent digital communications for underwater acoustic channels. *IEEE J. Ocean. Eng.* **1994**, *19*, 100–111.

15. Li, J.; Stoica, P.; Zheng, X. Signal synthesis and receiver design for MIMO radar imaging. *IEEE Trans. Signal Process.* **2008**, *56*, 3959–3968.

16. Song, A.; Badiey, M.; McDonald, V.K. Multi-Channel Combining and Equalization for UWA MIMO Channels. In Proceedings of IEEE Oceans Conference, Quebec City, QC, USA, 15–18 September 2008; pp. 1–6.

17. Real, G. Very High Frequency, MIMO Underwater Acoustic Communications in Ports and Shallow Waters. Master's Thesis, Florida Atlantic University, FL, USA, 2011.

18. Proakis, J.G. *Digital Communications*, 4th ed.; McGraw-Hill: New York, NY, USA, 2000.

19. Laot, C.; le Bidan, R.; Leroux, D. Low-complexity MMSE turbo equalization: a possible solution for EDGE. *IEEE Trans. Wirel. Commun.* **2005**, *4*, 965–974.

20. Medwin, H.; Clay, C.S. *Fundamentals of Acoustical Oceanography*; Academic Press: Waltham, MA, USA, 1997.